Environmental Science & Technology

pubs.acs.org/est

Article

Secondary Organic Aerosol Formation of Fleet Vehicle Emissions in China: Potential Seasonality of Spatial Distributions

Keren Liao, Qi Chen,* Ying Liu, Yong Jie Li, Andrew T. Lambe, Tong Zhu, Ru-Jin Huang, Yan Zheng, Xi Cheng, Ruqian Miao, Guancong Huang, Reza Bashiri Khuzestani, and Tianjiao Jia

Cite This: https://doi.org/10.1021/acs.est.0c08591

Read Online

ACCESS | Metrics & More | Article Recommendations | Supporting Information

ABSTRACT: Vehicle emissions are an important source of urban particular matter. To investigate the secondary organic aerosol (SOA) formation potential of real-world vehicle emissions, we exposed on-road air in Beijing to hydroxyl radicals generated in an oxidation flow reactor (OFR) under high-NO_x conditions on-board a mobile laboratory and characterized SOA and their precursors with a suite of state-of-the-art instrumentation. The OFR produced 10−170 $\mu g\ m^{-3}$ of SOA with a maximum SOA formation potential of 39−50 $\mu g\ m^{-3}\ ppmv^{-1}$ CO that occurred following an integrated OH exposure of (1.3−2.0) × 10^{11} molecules cm^{-3} s. The results indicate relatively shorter photochemical ages for maximum SOA production than previous OFR results obtained under low-NO_x conditions. Such timescales represent the balance of functionalization and fragmentation, possibly resulting in different spatial distributions of SOA in different seasons as the oxidant level changes. The detected precursors may explain as much as 13% of the observed SOA with the remaining plausibly contributed by the oxidation of undetected intermediate-volatility organic compounds. Extrapolation of the results suggests an annual SOA production rate of 0.78 Tg yr^{-1} from mobile gasoline sources in China, highlighting the importance of effective regulation of gaseous vehicular precursors to improve air quality in the future.

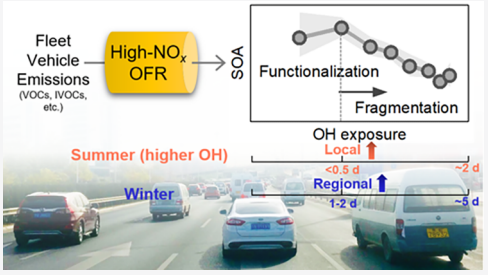

KEYWORDS: *mobile laboratory, vehicle emissions, oxidation flow reactor, high NO_x, SOA, spatial distributions*

1. INTRODUCTION

Particles having an aerodynamic diameter greater than 2.5 μm ($PM_{2.5}$) affect radiative forcing, visibility, and human health. Traffic emissions are an important source of $PM_{2.5}$ in urban areas. Vehicles emit primary particles such as primary organic aerosol (POA) and black carbon (BC) that contribute to about 6−37% of the $PM_{2.5}$ mass in urban environments globally.[1] Vehicles also emit gaseous inorganic and organic compounds that can form secondary aerosols following reaction with atmospheric oxidants such as hydroxyl (OH) radicals.[2] For example, OH oxidation of sulfur dioxide (SO_2) and nitrogen oxides (NO_x) generates sulfuric and nitric acid, which react with ammonia (NH_3) to form particulate sulfate, nitrate, and ammonium. Similarly, oxidation of volatile organic compounds (VOCs) and intermediate-volatility or semivolatile organic compounds (I/SVOCs) with saturation concentrations of >3 × 10^6 and (300−3) × 10^6/0.3−300 $\mu g\ m^{-3}$, respectively, produces secondary organic aerosol (SOA).[3]

Significant efforts have been made to characterize the SOA formation potential of VOCs and I/SVOCs that are present in motor vehicle emissions. Environmental chamber studies suggest that SOA concentrations obtained from atmospheric oxidation of these VOCs and I/SVOCs exceed POA concentrations over timescales that are relevant to local and regional transport with reported SOA-to-POA ratios ranging from 1 to >500.[2] Known SOA precursors in motor vehicle emissions include single-ring aromatics, long-chain alkanes, alkylcyclohexanes, polycyclic aromatic hydrocarbons (PAHs), and oxygenated VOCs (OVOCs). Some of the IVOCs (e.g., naphthalene (Nap), substituted naphthalenes, and C_7−C_{15} alkylbenzenes) have greater SOA yields than the single-ring aromatic precursors (e.g., benzene, toluene, and xylenes).[4−7] However, comprehensive characterization and speciation of atmospheric I/SVOCs are challenging, in part, because they mostly contribute to the unresolved complex mixture (UCM) that is present in traditional gas chromatography-based techniques.[8] The detection of oxygenated I/SVOCs presents additional analytical challenges.[8]

Attempts to extrapolate results from simplified laboratory chamber studies to complex, city-scale motor vehicle fleet emissions are exacerbated by mixed contributions from gasoline and diesel vehicles with a wide range of emission standards and control technologies. Emissions from old-type diesel and gasoline (e.g., pre-LEV in the United States) vehicles have similar SOA formation potential as unburned

Received: December 20, 2020
Revised: May 5, 2021
Accepted: May 5, 2021

Downloaded via PEKING UNIV on May 20, 2021 at 01:55:59 (UTC).
See https://pubs.acs.org/sharingguidelines for options on how to legitimately share published articles.

ACS Publications

© XXXX American Chemical Society

fuels.[9] Correspondingly, emissions from older diesel vehicles formed more SOA than gasoline vehicle emissions because of the heavier fuels.[10,11] On the other hand, modern diesel vehicles equipped with a diesel particle filter (DPF) and a diesel oxidation catalyst (DOC) produce much less POA and SOA than older ones without the after-treatment system.[12] Similar effective SOA yields were found for gasoline vehicles with different engine technologies and certification standards.[13] Gasoline vehicles that meet new stringent emission standards may therefore produce less SOA because of the reduced nonmethane organic gas (NMOG) emissions. However, real-world conditions introduce a factor of 3−50 variability in the SOA formation potential depending on the specific driving condition, e.g., hot/cold start or idle/cruise modes.[14,15] NO_x levels strongly affect the SOA formation from vehicle emissions.[10,11] Inconsistency of the reported SOA yields remains between the chamber and the OFR studies.[11,13] Thus, measurements of the SOA formation potential of mixed-fleet motor vehicle conditions under realistic driving conditions are urgently needed to provide inputs to chemical transport models.

One recent approach to addressing these issues involves the application of OFR to study the in situ oxidative aging of SOA precursors present in city-scale fleet vehicle emissions contributed by a range of vehicles, fuels, and operating modes.[16−18] The OFR experiments conducted in a US traffic tunnel suggest that vehicle-derived SOA may be 6 times greater than primary $PM_{2.5}$ vehicle emissions.[16] Similarly, roadside OFR experiments in Hong Kong suggest that vehicle-derived SOA exceeds primary $PM_{2.5}$ vehicle emissions in China by a factor of 3.5.[18] However, large uncertainties remain in the understanding of vehicle contributions to SOA because of the limited number of OFR-related studies of ambient vehicle fleet emissions to date and the lack of such studies under high-NO_x conditions. To build on these recent studies, we deployed an OFR on a mobile laboratory platform and conducted on-road, real-time measurements of the SOA formation potential of motor vehicle emissions in Beijing under high-NO_x conditions.

2. MATERIALS AND METHODS

The PKU mobile laboratory is built on an IVECO Turin V diesel vehicle.[19] On-board instruments are powered by two sets of uninterruptible power systems that have 192 V/100 Ah $LiFePO_4$ batteries, which allow a continuous operation of over 10 h at a full instrument load. Two types of OFR experiments were performed, including (1) mobile OFR experiments in November 2018 for eight nonhaze days and one haze day when the daily mean $PM_{2.5}$ mass concentration was over 75 $\mu g\ m^{-3}$ during 9:00 a.m. to 4:00 p.m. on the 4th ring road and (2) stationary OFR experiments during the nonhaze daytime in the Datunlu Tunnel (40.0089° N, 116.4074° E) on 20 February 2019 and by the roadside of the 4th Ring Road (39.9912° N, 116.3263° E) on 18−19 February 2019. Details about the sampling locations are provided in Section S1 and Figure S1 in the Supporting Information (SI). The average traffic volume on the 4th Ring Road was about 4000−8000 vehicles per hour, and more than 90% of the fleet consisted of light-duty gasoline vehicles (LDGVs) that meet National Stage III to V emission standards equivalent to Euro 3−5.

A suite of instruments was used during the mobile laboratory campaign (Figure S2 in the SI). An Aerodyne potential aerosol mass (PAM) OFR was used to generate OH and NO via photolysis of O_2, H_2O, and N_2O at λ = 185 nm and photolysis of O_3 at λ = 254 nm by four low-pressure mercury fluorescent lamps, which can be named as OFR185-iN_2O experiments.[20,21] Fluorescent dimming ballasts were used to regulate the current applied to the lamps. To achieve different OH concentrations in the OFR, the UV irradiance was varied by systematically changing the control voltage applied to the ballasts. Mass concentrations of nonrefractory $PM_{2.5}$ (NR-$PM_{2.5}$) species were measured by a capture vaporizer (CV)-based Aerodyne time-of-flight aerosol chemical speciation monitor (TOF-ACSM) with a time resolution of 40 s.[22] VOCs including OVOCs were measured by an Ionicon proton transfer reaction-quadrupole ion guide time-of-flight mass spectrometer (PTR-QiTOF) with a time resolution of 2 s.[23] Carbon dioxide (CO_2), nitrogen dioxide (NO_2), nitrogen oxides (NO), SO_2, carbon monoxide (CO), and ozone (O_3) were measured by gas analyzers (Licor LI-7500; Teledyne T500U; Ecotech 9841A, 9850A, 9830A, and 9810A, respectively). A weather station was mounted on the front top of the vehicle, which measures temperature and relative humidity (RH) (Rotronic, HC2-S3). Detailed information about instrument operation, calibration, and data analysis is provided in Section S2 and Tables S1 and S2 in the SI. VOC species detected by the PTR-QiTOF were categorized into several groups, including single-ring aromatics for benzene, toluene, C_8-aromatics, C_9-aromatics, and styrene; olefins for butenes, methylcyclopentenes, and methylcyclohexenes; C_2−C_4 carbonyls for acetaldehyde, acetone, and methyl ethyl ketone; PAHs for naphthalene, methylnaphthalene (MN), C_2-naphthalene, C_3-naphthalene, C_4-naphthalene, acenaphthene, fluorene, C_1-fluorene, phenanthrene or anthracene, C_1-phenanthrene or anthracene, C_2-phenanthrene or anthracene, fluoranthene or pyrene, and C_1-fluoranthene or pyrene; volatile chemical product (VCP) tracers for decamethylcyclopentasiloxane (D_5), dodecamethylcyclohexasiloxane (D_6), and parachlorobenzotriflouride; and other OVOCs for all detected OVOCs expect C_2−C_4 carbonyls (Table S2).[24]

Sampling inlets were installed in the front of the vehicle at 3.4 m above ground level (Section S3 in the SI). For ambient measurements, particles were sampled through a stainless steel cone-shape isokinetic inlet. The sampling flow then passed through a cyclone (URG, 2000−30EH) to remove coarse particles. The size-cut of the cyclone was about 2.5 μm at a flow rate of 15.9 L min^{-1}. VOCs were sampled through a Teflon line, and particles were removed from the PTR-QiTOF sample flow with an in-line Teflon filter. Other gas pollutants were sampled separately through a Teflon inlet line and then delivered to the inorganic gas analyzers via a glass manifold. Self-pollution from the vehicle exhaust during driving was minimized by positioning the exhaust exit to the back end and keeping the driving speed around 60 km h^{-1}. Above 30 km h^{-1}, the influence of mobile lab emissions on the concentrations of ambient gaseous pollutants became negligible (Figure S3 in the SI). The data that were collected at a speed of less than 30 km h^{-1} during occasional traffic jams have been removed from the analysis.

Over the range of OFR conditions that were used, the integrated OH exposure was calculated by measuring the decay of benzene and toluene present in ambient air using the PTR-QiTOF.[25] The OH exposure ranged approximately (1.0−5.6) × 10^{11} molecules cm^{-3} s. Corresponding equivalent photochemical aging timescales ranged from 0.8 to 4.3 days' exposure to an OH concentration of 1.5 × 10^6 molecules cm^{-3}.[26] The NO/HO_2 ratio ranged from approximately 2 to

https://doi.org/10.1021/acs.est.0c08591
Environ. Sci. Technol. XXXX, XXX, XXX−XXX

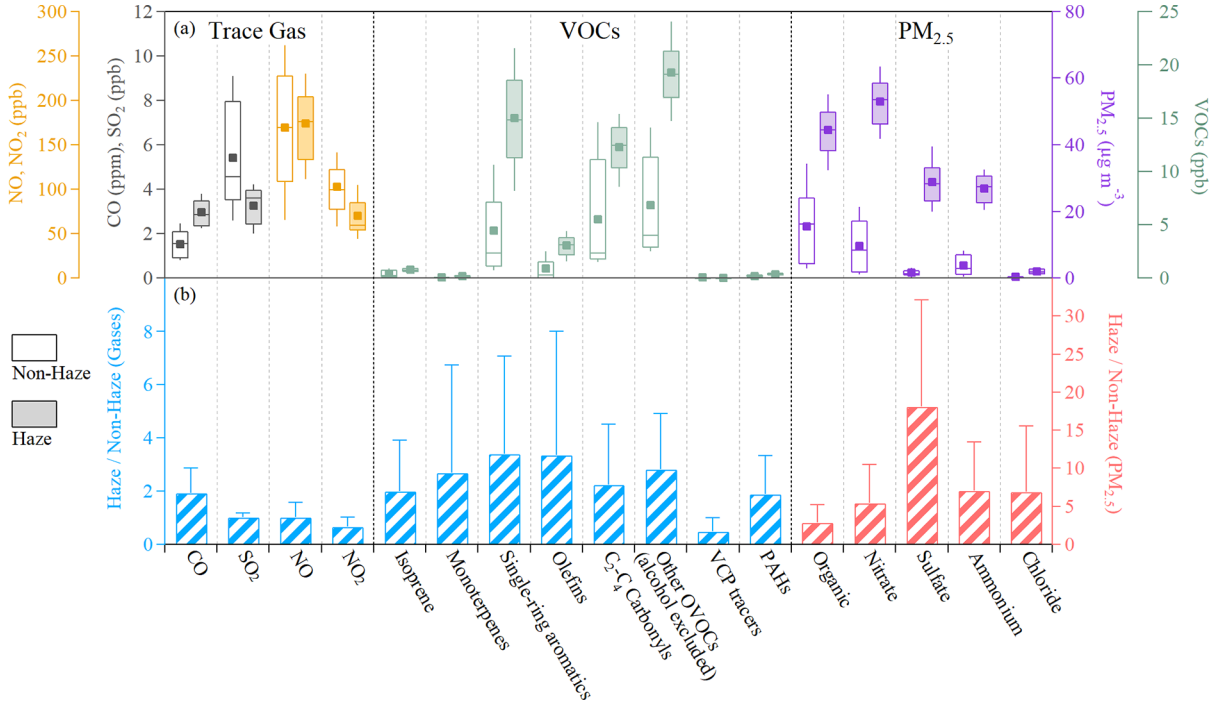

Figure 1. Results from ambient measurements on the 4th Ring Road of Beijing. The top row shows ambient concentrations of gaseous and particulate pollutants. The bottom row shows the concentration enhancements under haze conditions relative to nonhaze conditions. The box and whisker plots show the mean and median, 75th and 25th percentiles, and 90th and 10th percentiles. Error bars for the bar plots represent propagated standard deviations. VOC categories are described in the Materials and Methods section.

10, estimated by an OFR-based photochemical box model (Section S2).[20] Although the NO/HO_2 ratios in the OFR are lower than ambient conditions, a good high-NO condition can be achieved by the OFR185-iN_2O technique following the guidelines introduced by Peng et al.[21] The overall contribution of non-OH reactants to gas-phase chemistry including the VOC photolysis at 185 and 254 nm and the NO_3 chemistry should be negligible based on semiquantitative assessments by the Peng et al. toolkit.[27] The TOF-ACSM, PTR-QiTOF, and gas analyzers (except for CO) alternated sampling the OFR output (15 min) and the ambient bypass line (5 min) at 4.5 L min^{-1} every 20 min. When the instruments sampled the ambient bypass line, a 4.5 L min^{-1} makeup flow was pulled through the reactor to reduce stagnation and to decrease the re-equilibrium time after switching back to OFR sampling.

The SOA formation potential of ambient motor vehicle emissions is expressed as the ratio of the maximum absolute enhancement of OA (OA_{AE}) generated in the OFR to the background-subtracted mixing ratio of CO, assuming that CO represents a primary tracer for combustion whose reaction with OH is slow over typical regional transport timescales.[28,29] Previous studies often use the CO concentrations measured at upwind or nearby relatively clean sites as the background CO levels.[16−18] For the mobile measurements (17 km × 18 km) herein, it is difficult to determine the background site. We therefore derived the correlation slopes between OA_{AE} and $CO_{measured}$ as statistically meaningful $\Delta OA_{AE}/\Delta CO$ (Section S4 in the SI).[30] Only nonhaze on-road data were used for this calculation because the SOA potential (SOAP) can be significantly affected by sources other than vehicle emissions during the haze events. We assume that on-road gas pollutants (CO and SOA precursors) are mainly from vehicle emissions during nonhaze days in winter in Beijing because major industry and power plants have been relocated out of the capital area. Nearby low-intensity local sources such as restaurants and off-road engines are expected to have little impact on the on-road measurements with a driving speed of 60 km h^{-1} over the city. For stationary measurements, the influence might be large during episode periods depending on the speed and direction of surface wind, and thus, we only used those measurements for comparisons of known precursor contributions. OA_{AE} and CO were grouped by 0.5-day equivalent photochemical age, and the regressions were conducted by the reduced major axis method.

Contributions of known SOA precursors to the measured OA_{AE} were calculated from their oxidative loss in the OFR with corresponding SOA yields obtained from the OH oxidation of these precursors in environmental chamber studies.[4,5,31] Some SOA precursors lack yield parameterizations, for which we used the SOA potential (SOAP)[32] and the fractional aerosol coefficient (FAC) methods[33] to estimate their contributions to the measured OA_{AE} in the OFR instead. Section S5 and Tables S3 and S5 in the SI provide details about the methods and parameters used herein. The SOA yields were calculated for the OA concentrations measured downstream of the OFR at the mean ambient temperature of the measurement periods. OA_{AE} values have been corrected for particle wall losses in the OFR, which are approximately 10% (Figure S5 in the SI).

3. RESULTS AND DISCUSSION

3.1. Primary Emissions. Figure 1 shows on-road ambient concentrations of particulate and gaseous pollutants measured during this study. The mean mixing ratios of CO and NO_x during nonhaze days are a factor of 2 higher than CO and NO_x levels observed at urban and suburban sites in Beijing, largely contributed by the on-road traffic emissions.[34,35] The mean SO_2 mixing ratio of 5.4 ± 2.4 (±1 σ) ppb is lower than

https://doi.org/10.1021/acs.est.0c08591
Environ. Sci. Technol. XXXX, XXX, XXX−XXX

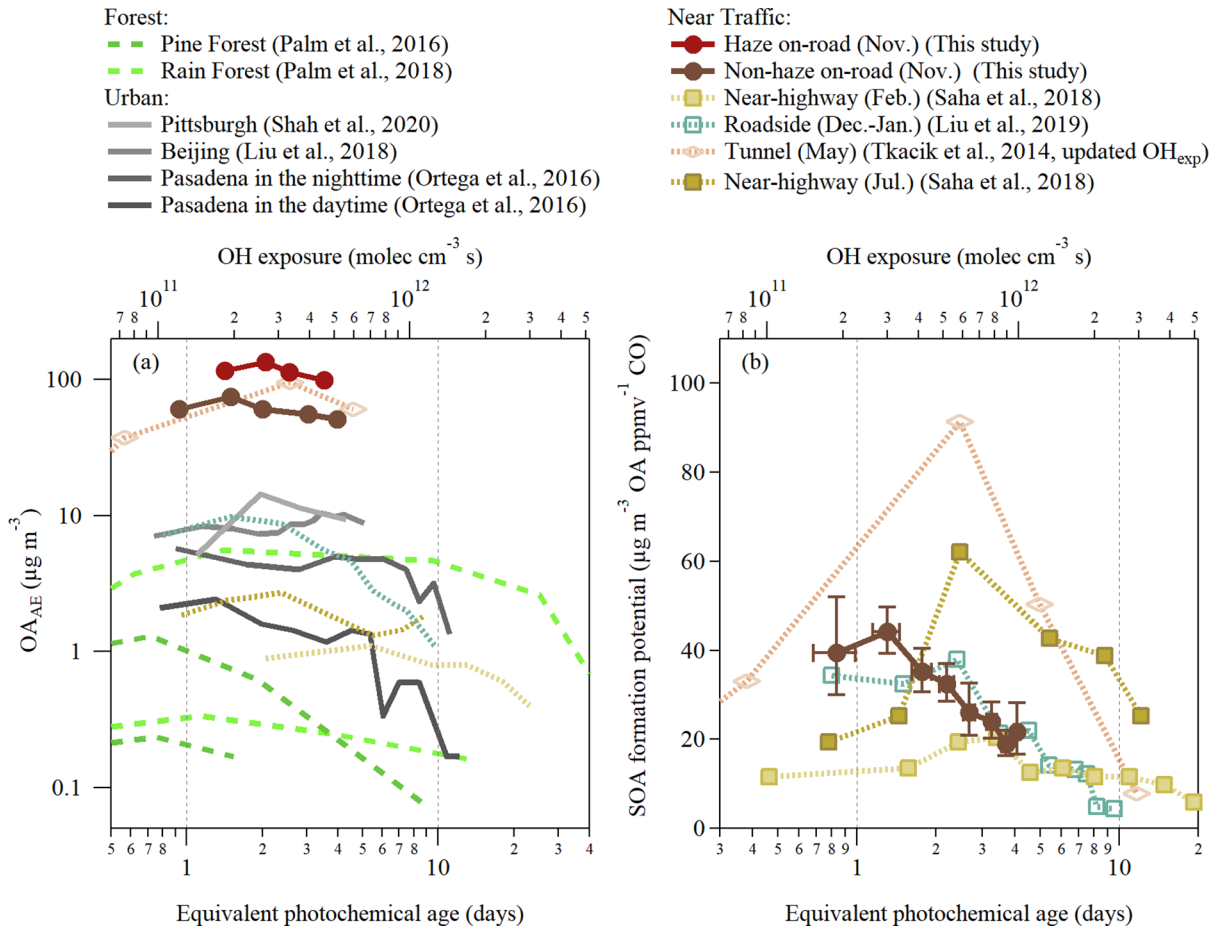

Figure 2. (a) OA_{AE} obtained by the OFR experiments in ambient environments and (b) SOA formation potential corresponding to the near-traffic sources under different OH exposures. OH exposure is shown as equivalent atmospheric age, assuming a daily mean OH concentrations of 1.5×10^6 molecules cm^{-3}. Updated OH_{exp} for results of Tkacik et al.[16] are taken from Figure S3 in the study of Gentner et al.[2] Only the upper- and lower-bound OA_{AE} values in Palm et al.[53] are shown. For our study, only on-road data were used in panel (a) and only nonhaze data were used to calculate the SOA formation potential in panel (b). In panel (b), error bars on the SOA potential represent the 95% confidence intervals of the regression slopes between OA_{AE} and CO (Section S4) and error bars on equivalent photochemical age represent the standard deviations.

previous findings in Beijing (10.2 ± 7.3 ppb), which is consistent with the emission regulations that led to an annual reduction rate of ~19% for anthropogenic SO_2 from 2013 to 2018 in China.[36,37] During the severe-haze measurement period, the mean concentration of CO increased from 1.5 to 3.0 ppm, whereas the concentrations of NO were similar to those measured during the nonhaze periods. This suggests that our measurements were influenced by nonvehicular combustion sources during the severe-haze period. The SO_2 mixing ratios show no significant enhancement during the severe-haze period compared to the clean case, which may be explained by the large conversion of gaseous SO_2 to sulfate by photochemical and aqueous processes.[34] The average mass concentrations of NR-$PM_{2.5}$ were 30.7 ± 24.7 and 155 ± 27 $\mu g\ m^{-3}$ for the nonhaze and severe-haze days, respectively. NR-$PM_{2.5}$ was dominated by OA and nitrate, which is consistent with previous urban-site observations.[38,39] Concentrations of particulate nitrate, sulfate, ammonium, and chloride were each enhanced by a factor of 5 (nitrate) to 18 (sulfate) during the severe-haze period relative to nonhaze days, on which heterogeneous or aqueous chemistry may play an important role (Figures 1b and S6). Meanwhile, the mass concentrations of OA were elevated by a factor of 3, of which about 62% of the increase was perhaps contributed by SOA as indicated by the positive matrix factorization (PMF) analysis of OA.[22] Details about the PMF analysis are provided in Section S2.2 in the SI.

Analytes measured with PTR-QiTOF were dominated by OVOCs and single-ring aromatic compounds, and their concentrations were enhanced by up to a factor of 4 during the severe-haze measurement period. Isoprene concentrations are higher than typical concentrations observed in urban environments,[35,40] potentially because of high isoprene emissions from Chinese motor vehicles.[41] Largely elevated isoprene concentrations during heavy traffic periods and concurrent plumes of isoprene along with benzene and toluene indicate that the measured isoprene was mainly contributed by vehicle emissions. The toluene-to-benzene (T/B) ratio was 1.6 ± 0.5 during nonhaze measurement periods, which is consistent with the T/B ratio of 1.5−3.0 for fresh vehicle emissions.[42−44] During the severe-haze period, the T/B ratio became lower (1.3 ± 0.5), explained by faster OH oxidation of toluene than benzene present in regionally transported air masses that contributed to the haze.[45] Concentrations of tracers for VCPs that are emitted from noncombustion sources are significantly lower in Beijing than in Pittsburgh and New York, highlighting the possibility of relatively low usage of such products in China.[46]

https://doi.org/10.1021/acs.est.0c08591
Environ. Sci. Technol. XXXX, XXX, XXX−XXX

Table 1. Maximum SOA Potential and the Corresponding Equivalent Photochemical Age at [OH] = 1.5 × 10^6 Molecules cm^{-3} for Traffic Sources

sampling location		maximum SOA potential ($\mu g\ m^{-3}$ OA $ppmv^{-1}$ CO)[b] [maximum SOA potential corrected for LVOC loss]	LVOC fates: fraction of condensing onto aerosols	equivalent photochemical age (days)	vehicle type	reference
tunnel (spring: 16 °C[a])		91 (64−151)[c]	>90%[f]	2−3	90−96% light-duty vehicles (mainly gasoline-fueled)	Tkacik et al.[16]
on-road (winter: 8 °C)		44 (39−50)[d]	>95%	1−1.5	>90% light-duty gasoline vehicles	this study[g]
roadside	1 m away from a major road (winter: 18 °C)	38 ± 65[e] [48]	50−80%	2−3	40.8% gasoline, 30.3% diesel, and 28.9% liquefied petroleum gas vehicles	Liu et al.[18]
	10 m away from a highway (winter: 6 °C)	20 [110]	<30%	3−4	∼95% light-duty vehicles	Saha et al.[17]
	10 m away from a highway (summer: 26 °C)	62 ± 18[e] [180]	<40%	2−3	∼95% light-duty vehicles	Saha et al.[17]

[a]Mean temperature during the measurement period. [b]Uncorrected for vapor wall loss. [c]The 25th to 75th percentile of the results. [d]The 95% confidence intervals of the regression slopes. [e]Standard deviation of the results. [f]Roughly estimated based on the studies of Li et al.[76] and Ahlberg et al.[61] [g]Only for nonhaze days.

3.2. Potential SOA Formation. Following exposure to OH radicals in the OFR, concentrations of ambient VOCs (e.g., single-ring aromatic compounds) decreased and concentrations of OVOCs (e.g., acetic acid and acetaldehyde) and OA increased (Figure S7). The OA concentrations generated in the OFR ranged from 10 to 170 $\mu g\ m^{-3}$ during the campaign in contrast with ambient concentrations of 2.5−80 $\mu g\ m^{-3}$ (Figure 1a). The concentrations of sulfate showed a small change of less than 10 $\mu g\ m^{-3}$ after the OFR exposure, which is consistent with the low concentrations of SO_2 in the sampling air. The mass concentrations of ammonium and nitrate increased by 5−100 $\mu g\ m^{-3}$ due to the thermodynamic equilibrium of ambient NH_3 and HNO_3 that was generated in the OFR following the reactions of NO + O_3 → NO_2 + O_2 and NO_2 + OH → HNO_3, including both contributions of ambient NO_x and OFR NO_x originated from N_2O. Based on the photochemical box model, we roughly estimated that approximately 10% of the HNO_3 was generated from ambient NO_x with the remaining HNO_3 originating from NO_x generated in the OFR by N_2O photolysis.[20] Similar to the tunnel study in Pittsburgh,[16] NH_3 emitted from gasoline vehicles was sufficient to neutralize the particle-phase nitrate (Figure S8 in the SI). Sun et al. show on-road NH_3 concentrations of 20−40 ppb in Beijing.[47] Under rich ammonia conditions, the formation of ammonium nitrate is perhaps sensitive to HNO_3 availability, highlighting the importance of mobile source contribution to nitrate.[48]

Figure 2a shows OA_{AE} as a function of OH exposure observed in this study and in previous OFR studies obtained in urban,[49−51] forest,[52,53] and near-traffic environments.[16−18] Depending on the composition and concentration of SOA precursors, OA_{AE} may vary considerably even in the same kind of environment. Various and abundant precursors typically present in urban environments, leading to greater OA_{AE} than in forests.[49−51] Notably, we observed OA_{AE} of 50−75 $\mu g\ m^{-3}$ during nonhaze periods and OA_{AE} > 100 $\mu g\ m^{-3}$ during the severe-haze period on road in Beijing. These OA_{AE} values are a factor of 5−500 higher than OA_{AE} observed in previous urban and forested OFR studies. The large OA_{AE} is presumably due to our close proximity to motor vehicle emissions, enabling high concentrations of anthropogenic SOA precursors with potentially high SOA yields to be sampled into the OFR, whereas other studies with lower OA_{AE} are conducted further from sources and thus sampled ambient air that had been subjected to more dilution or contained lower SOA formation potential.

OA_{AE} values initially increase with increasing OH exposure and then decrease above an equivalent photochemical age of approximately 1−2 days in a manner that is qualitatively consistent with the other studies shown in Figure 2a where peak OA_{AE} values are over 1−4 days of equivalent atmospheric OH oxidation. This trend reflects a transition from oxidative aging conditions that initially favor the addition of oxygen-containing functional groups to the carbon backbone of the SOA precursors, thereby increasing the yield of SOA (i.e., so-called "functionalization") prior to carbon−carbon bond cleavage with continued OH exposure that decreases the SOA yield ("fragmentation").[54−56] In general, a net loss of 20−90% of the peak OA_{AE} may occur beyond 10 days of equivalent photochemical age ([OH] = 1.5 × 10^6 molecules cm^{-3}).

Figure S9 in the SI shows the mass spectra and the variations of OA factors that are identified by the PMF analysis on the CV-based OA spectra. Two primary OA factors were resolved and labeled as HOA (i.e., hydrocarbon-like OA) and COA (i.e., cooking OA), and three oxygenated OA factors were labeled as OOA1, OOA2, and OOA3, for which the suffixes 1, 2, and 3 signify ordinal ranking with respect to the extent of oxidation from low to high (Figure S9a). The mass concentration of HOA decreased, whereas the concentrations of the three OOAs increased after exposed to OH in OFR (Figure S9b). COA show insignificant changes in concentration, suggesting possibly much slower heterogeneous aging than HOA. The increase and later decrease of the mass fraction of OOA3 in OA with increasing OH exposure are consistent with the evolution from functionalization to fragmentation, which is similar to that observed in atmospheric aging of OA.[56] Fragmentation may explain the earlier increase of the more oxidized OOA3 than the less oxidized OOA2 as well as the reverse change of their mass fraction at the photochemical age of 3 days. At high OH exposure, fragmentation becomes more important in product formation. The less oxidized OOA2 perhaps represents fragmented condensable products.

https://doi.org/10.1021/acs.est.0c08591
Environ. Sci. Technol. XXXX, XXX, XXX−XXX

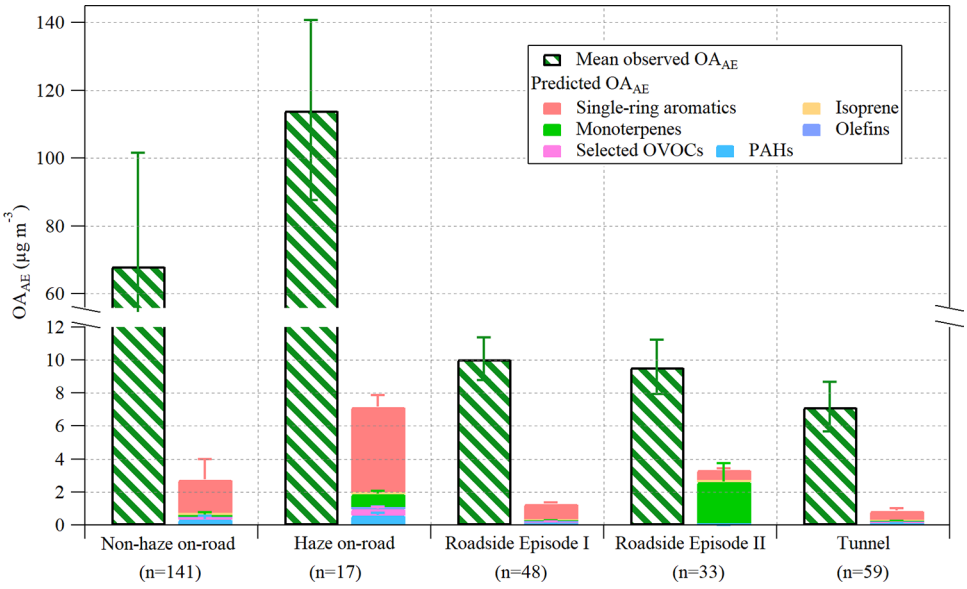

Figure 3. Mean observed OA_{AE} corresponding to the equivalent photochemical age of 1.5 ± 0.2 days and the predicted OA_{AE} contributed from OH oxidation of precursors measured with PTR-QiTOF. Error bars show the standard deviations of the data for each case with the sample size shown as *n* below. VOC categories are described in the Materials and Methods section. Selected OVOCs include CH_3OH, C_2H_6O, C_4H_8O, $C_4H_8O_2$, C_5H_6O, C_6H_6O, and $C_8H_{10}O$.

Figure 2b shows the SOA formation potential ($\Delta OA_{AE}/\Delta CO$) of traffic emissions as a function of OH exposure. The maximum SOA formation potential of 44 (39−50 corresponding to the 95% confidence intervals of the regressions in Figure S10 in the SI) $\mu g\ m^{-3}$ OA $ppmv^{-1}$ CO occurred at 1−1.5 days of equivalent photochemical age (see Section S4 for details). The loss of low-volatility organic compounds (LVOC) estimated by the fate model of Palm et al. is less than 5% (Figure S11 in the SI).[52] This $\Delta OA_{AE}/\Delta CO$ value falls within the envelope of maximum $\Delta OA_{AE}/\Delta CO$ of 20−91 $\mu g\ m^{-3}$ (48−180 $\mu g\ m^{-3}$ corrected for LVOC loss) OA $ppmv^{-1}$ CO values observed in previous OFR studies on motor vehicle emissions (Table 1). Factors that may contribute to the spread in observed $\Delta OA_{AE}/\Delta CO$ values across the different studies include (1) ambient temperature, (2) vapor wall losses in the OFR, (3) vehicle fleet composition, and (4) photochemical conditions (e.g., NO_x conditions). We discuss each of these factors below.

Ambient temperature may affect SOA formation by altering engine combustion conditions or the gas-particle partitioning of semivolatile species.[57] Incomplete combustion on cold starts may lead to greater emissions at lower temperatures.[8,13,58−60] In this study, the fleet emissions represent mainly hot-running conditions. The temperature effects on the SOA formation are therefore more likely related to the shifts in gas-particle partitioning rather than the differences in engine operations.[8,13,58,60] Lower temperatures may favor the condensation of semivolatile compounds, thereby potentially reducing the concentrations of primary emissions available for OH oxidation, but increase the SOA yields by favoring the condensation of oxidation products that are formed.[57] For a temperature change from 26 to 6 °C (Table 1), the former reduction of the precursor emissions is perhaps a few percent,[8] while the increase of SOA yields is expected to be more significant (e.g., ∼90% increase of the yield for benzene). The net effect is enhanced SOA formation potential at lower temperatures. However, the two highest $\Delta OA_{AE}/\Delta CO$ values (i.e., 62 and 91 $\mu g\ m^{-3}$ OA $ppmv^{-1}$ CO) were obtained at relatively high ambient temperatures (Table 1). We therefore conclude that temperature is unlikely the primary factor governing the spread in $\Delta OA_{AE}/\Delta CO$ values summarized in Table 1.

Vapor wall losses in OFRs potentially reduce the amount of material available for OH oxidation or condensation.[52] Unaccounted-vapor wall loss may contribute to some of the spread in reported $\Delta OA_{AE}/\Delta CO$ values across the different OFR experiments.[61] The calculated upper-limit vapor wall loss in near-road OFR studies ranged from <5 to 70%. The LVOC loss depends largely on the particle size distributions. Our study and the tunnel study in Pittsburgh have much greater particle surface area concentrations than the other roadside studies and therefore negligible LVOC loss. The wintertime $\Delta OA_{AE}/\Delta CO$ of 20 $\mu g\ m^{-3}$ $ppmv^{-1}$ CO reported by Saha et al.[17] has the highest calculated vapor wall loss fraction of >70%. For such cases, the correction of LVOC loss may introduce a large uncertainty.

The motor vehicle fleet composition affects the measured SOA formation potential because SOA yields are precursor-dependent. Different countries have different vehicle types, emission standards, and after-treatment devices, potentially resulting in different emission factors of specific SOA precursors.[2] Figure S12 in the SI compares VOC/benzene and IVOC/benzene emission factors in LDGV-dominant fleets characterized in this study and in a tunnel study in Pittsburgh.[16,16] Concentrations of Nap and MN are about 14−84 ppt (25th−75th percentiles; the same below) in Pittsburgh and 0−32 ppt in Beijing, with corresponding Nap/benzene and MN/benzene ratios of 0.37 and 0.20 in Pittsburgh and 0.04−0.26 and 0−0.11 in Beijing. Thus, higher $\Delta OA_{AE}/\Delta CO$ values in the US studies might be partially explained by the greater emissions of Nap and MN that have high SOA yields, even though the Chinese vehicle fleet sampled in this study contained higher emissions of VOCs such as isoprene that have low SOA yields. Notably, recent studies suggest that the effects of vehicle technologies on the composition of gasoline vehicle emissions are small, although

https://doi.org/10.1021/acs.est.0c08591
Environ. Sci. Technol. XXXX, XXX, XXX−XXX

there may be a small enhancement of IVOC emissions relative to NMOG emissions from the new-type vehicles.[10,11,13,60,62,63]

Moreover, the measurements described herein are the first ambient OFR study to incorporate N_2O to generate NO at levels that can compete with HO_2 for reaction with organic radicals (RO_2). This different photochemical regime may result in different SOA chemistry than in previous urban OFR measurements where $RO_2 + HO_2$ and $RO_2 + RO_2$ reactions were the primary RO_2 loss pathways.[64] The lower signal ratios of m/z 46:30 (i.e., NO_2^+/NO^+) for particles out of OFR than the ratios for ambient particles and pure ammonium nitrate suggest the enhancement of organonitrates in the reactor resulting from the RO_2 + NO pathway (Figure S13 in the SI).[22,65] We also observed enhanced formation of nitrophenol in the OFR by PTR-QiTOF, which confirms the high-NO_x conditions in the reactor (Figure S14 in the SI). Chamber and OFR experiments have shown different SOA production levels of gasoline vehicle emissions under different NO_x conditions.[10,11,13,66] NO_x conditions might be an important reason for the spread in $\Delta OA_{AE}/\Delta CO$ values in Table 1.

The equivalent photochemical ages corresponding to the maximum SOA formation potential range from 1 to 4 days (Table 1). The equivalent photochemical age corresponding to the maximum SOA formation potential reflects the timescale to balance the functionalization and fragmentation, which may determine the spatial distribution of the SOA production from vehicle emissions. Factors that contribute to this spread may include (1) photochemical conditions in the OFR (e.g., NO_x conditions that were discussed above), (2) SOA precursor structure and OH reactivity, and (3) uncertainty in the calculated OH exposure. For instance, first-generation products contribute predominantly to the SOA mass for some precursors like single-ring aromatics and naphthalene,[4,5] for which the timescale of maximum SOA production is perhaps determined by the reaction rates of precursors with OH and varies by precursors.[67] On the other hand, delayed timescales of maximum SOA production are expected for cases involving multigeneration contribution to SOA (e.g., the oxidation of some *n*-alkanes).[67,68] We further note that our use of online benzene and toluene measurements likely reduces associated uncertainty to calculated OH exposure values relative to previous studies that relied on offline OH exposure calibrations.[16−18]

Figure 3 compares the observed OA_{AE} values in this study for the equivalent photochemical age of 1.5 ± 0.2 days with the corresponding OA_{AE} values calculated from the OH oxidation of known SOA precursor classes that were measured with the PTR-QiTOF. The contribution of PTR-speciated compounds to observed OA_{AE} ranged from 4 to 13% and in most cases is dominated by aromatic compounds, aside from roadside episode II, during which the SOA formation potential of speciated monoterpenes exceeded that of the aromatics. Unlike the on-road measurements, the roadside measurements might be influenced by nearby local sources. PTR-speciated OVOCs (including C_1-C_2 alcohols, C_4-C_6 acetates, C_6-C_8 phenols, and benzaldehyde) contributed <1% of the observed OA_{AE} based on their assumed SOA formation potential. For unspeciated OVOCs (or fragments) up to m/z 500, the signals measured by PTR-QiTOF either increase or show negligible losses in the OFR, which unlikely contribute to a significant amount of the observed SOA. We hypothesize that IVOCs, e.g., linear alkanes, cycloalkanes, alkenes, and ethyl- and propyl-substituted aromatics, that the PTR-QiTOF is insensitive to, contribute the majority of the remaining unexplained OA_{AE}.[24] Consistently, a recent chassis dynamometer study on China Stage V gasoline vehicles shows that 80% of the SOA formed from the exhaust oxidation was contributed by IVOCs.[69]

4. ATMOSPHERIC IMPLICATIONS

The OA:CO-based parameterization is commonly used in chemical transport models to simulate the SOA production from combustion sources.[70,71] We obtained a maximum SOA formation potential of 44 (39−50) $\mu g\ m^{-3}$ OA $ppmv^{-1}$ CO for the fleet emissions in Beijing under high-NO_x conditions. We assume that the fleet composition in Beijing (i.e., a mixture of National Stage III−V vehicles for 90% of the fleet) is similar to other cities considering the intensive increase in the number of vehicles in operation nationwide in China in the past 10 years. The CO emissions from the transportation sector were 25.2 Tg in 2017 in China,[37] and about 88% of these CO emissions were contributed by gasoline vehicles according to the China Mobile Source Environmental Management Annual Report of 2019. With these values, we roughly estimate an annual SOA production rate of 0.78 (0.69−0.89) Tg yr^{-1} in China from mobile gasoline sources. This annual production rate is almost 52 times higher than the mobile gasoline primary $PM_{2.5}$ emissions in the Multiresolution Emission Inventory for China (MEIC).[37,72] By contrast, the PMF analysis herein indicates that the mass ratio of OOA (i.e., OOA1 + OOA2 + OOA3) to HOA is 8 ± 11 for 1−1.5 days of equivalent photochemical age, highlighting the importance of SOA production from mobile gasoline sources and the possibility of underestimation of traffic-related POA in the inventory. Moreover, NO_x and NH_3 associated with mobile sources contribute additional particulate inorganic nitrate. Despite effective reductions in SO_2 and NO_x emissions in the past 10 years,[37] the mass concentrations of SOA and nitrate in $PM_{2.5}$ remain high.[73] Observations underscore the importance of effective regulation of gas-phase precursors in vehicle emissions to directly reduce secondary aerosol formation in the future, even as car emissions and ozone levels are reduced.

The shorter equivalent photochemical age for reaching the maximum $\Delta OA_{AE}/\Delta CO$ in this study may point to the potential role of NO in competing with HO_2 for reaction with RO_2, thereby decreasing the OH exposure that is required to achieve maximum SOA formation, although other factors like precursor composition may also contribute. To the extent that the high-NO_x photochemical conditions in the OFR measurements herein mimic the oxidative aging processes that present in Beijing and other polluted cities, the maximum SOA potential would occur over an ambient timescale less than 1−1.5 days for a mean OH concentration of 1.5×10^6 molecules cm^{-3}. In Beijing, the daily maximum OH concentrations during clean episodes may reach 10^7 molecules cm^{-3} in summer and 2×10^6 molecules cm^{-3} in winter.[74,75] Thus, the integrated OH exposure may vary by about a factor of 5 across different seasons, suggesting seasonal atmospheric transport time for achieving maximum SOA formation potential. The influence of secondary pollution from mobile sources is plausibly local in summer. By contrast, the maximum SOA formation possibly occurs after a couple of days of aging, which is more relevant to regional transport in winter. Further reduction of vehicle emissions may localize the SOA formation in urban environments as emission controls improve. Chemical transport models assume a default timescale of 1 day for

https://doi.org/10.1021/acs.est.0c08591
Environ. Sci. Technol. XXXX, XXX, XXX−XXX

anthropogenic SOA formation processes,[71] which can introduce unclear spatial uncertainties depending on the actual OH exposure in different seasons. Further investigations are needed to better understand the links between the oxidative timescales and the resulting spatial distribution of SOA in polluted areas.

■ ASSOCIATED CONTENT

Supporting Information

The Supporting Information is available free of charge at https://pubs.acs.org/doi/10.1021/acs.est.0c08591.

Sampling locations, measurement details, mobile laboratory setup, determination of $\Delta OA_{AE}/\Delta CO$, SOA yield determination, self-contamination test, offline calibrations of the OFR, wall loss experiments, time series of an OFR experiment, ammonium balance, PMF results, LVOC fate analysis, VOC comparisons, NO_2^+/NO^+ ratios, and nitrophenol formation (PDF)

■ AUTHOR INFORMATION

Corresponding Author

Qi Chen − *State Key Joint Laboratory of Environmental Simulation and Pollution Control, BIC-ESAT and IJRC, College of Environmental Sciences and Engineering, Peking University, Beijing 100871, China;* orcid.org/0000-0003-3559-8914; Email: qichenpku@pku.edu.cn

Authors

Keren Liao − *State Key Joint Laboratory of Environmental Simulation and Pollution Control, BIC-ESAT and IJRC, College of Environmental Sciences and Engineering, Peking University, Beijing 100871, China*

Ying Liu − *State Key Joint Laboratory of Environmental Simulation and Pollution Control, BIC-ESAT and IJRC, College of Environmental Sciences and Engineering, Peking University, Beijing 100871, China;* orcid.org/0000-0001-5139-0211

Yong Jie Li − *Department of Civil and Environmental Engineering, Faculty of Science and Technology, University of Macau, Taipa, Macau 999078, China;* orcid.org/0000-0002-7631-9136

Andrew T. Lambe − *Aerodyne Research, Inc., Billerica, Massachusetts 01821, United States;* orcid.org/0000-0003-3031-701X

Tong Zhu − *State Key Joint Laboratory of Environmental Simulation and Pollution Control, BIC-ESAT and IJRC, College of Environmental Sciences and Engineering, Peking University, Beijing 100871, China;* orcid.org/0000-0002-2752-7924

Ru-Jin Huang − *State Key Laboratory of Loess and Quaternary Geology, Center for Excellence in Quaternary Science and Global Change, and Key Laboratory of Aerosol Chemistry & Physics, Institute of Earth Environment, Chinese Academy of Sciences, Xi'an 710075, China;* orcid.org/0000-0002-4907-9616

Yan Zheng − *State Key Joint Laboratory of Environmental Simulation and Pollution Control, BIC-ESAT and IJRC, College of Environmental Sciences and Engineering, Peking University, Beijing 100871, China*

Xi Cheng − *State Key Joint Laboratory of Environmental Simulation and Pollution Control, BIC-ESAT and IJRC, College of Environmental Sciences and Engineering, Peking University, Beijing 100871, China*

Ruqian Miao − *State Key Joint Laboratory of Environmental Simulation and Pollution Control, BIC-ESAT and IJRC, College of Environmental Sciences and Engineering, Peking University, Beijing 100871, China*

Guancong Huang − *State Key Joint Laboratory of Environmental Simulation and Pollution Control, BIC-ESAT and IJRC, College of Environmental Sciences and Engineering, Peking University, Beijing 100871, China*

Reza Bashiri Khuzestani − *State Key Joint Laboratory of Environmental Simulation and Pollution Control, BIC-ESAT and IJRC, College of Environmental Sciences and Engineering, Peking University, Beijing 100871, China*

Tianjiao Jia − *State Key Joint Laboratory of Environmental Simulation and Pollution Control, BIC-ESAT and IJRC, College of Environmental Sciences and Engineering, Peking University, Beijing 100871, China*

Complete contact information is available at: https://pubs.acs.org/10.1021/acs.est.0c08591

Notes

The authors declare no competing financial interest.

■ ACKNOWLEDGMENTS

This work was supported by the National Natural Science Foundation of China (Grant No. 91544107, 41875165, 51861135102, and 41961134034) and the 111 Project of Urban Air Pollution and Health Effects (B20009). The authors gratefully acknowledge Meng Wang, Yingjun Liu, and Zhe Peng for helpful discussion.

■ REFERENCES

(1) Karagulian, F.; Belis, C. A.; Dora, C. F. C.; Pruss-Ustun, A. M.; Bonjour, S.; Adair-Rohani, H.; Amann, M. Contributions to cities' ambient particulate matter (PM): A systematic review of local source contributions at global level. *Atmos. Environ.* **2015**, *120*, 475−483.

(2) Gentner, D. R.; Jathar, S. H.; Gordon, T. D.; Bahreini, R.; Day, D. A.; El Haddad, I.; Hayes, P. L.; Pieber, S. M.; Platt, S. M.; de Gouw, J.; Goldstein, A. H.; Harley, R. A.; Jimenez, J. L.; Prevot, A. S. H.; Robinson, A. L. Review of urban secondary organic aerosol formation from gasoline and diesel motor vehicle emissions. *Environ. Sci. Technol.* **2017**, *51*, 1074−1093.

(3) Donahue, N. M.; Kroll, J. H.; Pandis, S. N.; Robinson, A. L. A two-dimensional volatility basis set - Part 2: Diagnostics of organic-aerosol evolution. *Atmos. Chem. Phys.* **2012**, *12*, 615−634.

(4) Chan, A. W. H.; Kautzman, K. E.; Chhabra, P. S.; Surratt, J. D.; Chan, M. N.; Crounse, J. D.; Kurten, A.; Wennberg, P. O.; Flagan, R. C.; Seinfeld, J. H. Secondary organic aerosol formation from photooxidation of naphthalene and alkylnaphthalenes: Implications for oxidation of intermediate volatility organic compounds (IVOCs). *Atmos. Chem. Phys.* **2009**, *9*, 3049−3060.

(5) Ng, N. L.; Kroll, J. H.; Chan, A. W. H.; Chhabra, P. S.; Flagan, R. C.; Seinfeld, J. H. Secondary organic aerosol formation from m-xylene, toluene, and benzene. *Atmos. Chem. Phys.* **2007**, *7*, 3909−3922.

(6) Presto, A. A.; Miracolo, M. A.; Donahue, N. M.; Robinson, A. L. Secondary organic aerosol formation from high-NOx photo-oxidation of low volatility precursors: n-Alkanes. *Environ. Sci. Technol.* **2010**, *44*, 2029−2034.

(7) Zhao, Y. L.; Nguyen, N. T.; Presto, A. A.; Hennigan, C. J.; May, A. A.; Robinson, A. L. Intermediate volatility organic compound emissions from on-road gasoline vehicles and small off-road gasoline engines. *Environ. Sci. Technol.* **2016**, *50*, 4554−4563.

(8) Lu, Q. Y.; Zhao, Y. L.; Robinson, A. L. Comprehensive organic emission profiles for gasoline, diesel, and gas-turbine engines including intermediate and semi-volatile organic compound emissions. *Atmos. Chem. Phys.* **2018**, *18*, 17637−17654.
(9) Gentner, D. R.; Isaacman, G.; Worton, D. R.; Chan, A. W. H.; Dallmann, T. R.; Davis, L.; Liu, S.; Day, D. A.; Russell, L. M.; Wilson, K. R.; Weber, R.; Guha, A.; Harley, R. A.; Goldstein, A. H. Elucidating secondary organic aerosol from diesel and gasoline vehicles through detailed characterization of organic carbon emissions. *Proc. Natl. Acad. Sci. U.S.A.* **2012**, *109*, 18318−18323.
(10) Gordon, T. D.; Presto, A. A.; Nguyen, N. T.; Robertson, W. H.; Na, K.; Sahay, K. N.; Zhang, M.; Maddox, C.; Rieger, P.; Chattopadhyay, S.; Maldonado, H.; Maricq, M. M.; Robinson, A. L. Secondary organic aerosol production from diesel vehicle exhaust: impact of aftertreatment, fuel chemistry and driving cycle. *Atmos. Chem. Phys.* **2014**, *14*, 4643−4659.
(11) Gordon, T. D.; Presto, A. A.; May, A. A.; Nguyen, N. T.; Lipsky, E. M.; Donahue, N. M.; Gutierrez, A.; Zhang, M.; Maddox, C.; Rieger, P.; Chattopadhyay, S.; Maldonado, H.; Maricq, M. M.; Robinson, A. L. Secondary organic aerosol formation exceeds primary particulate matter emissions for light-duty gasoline vehicles. *Atmos. Chem. Phys.* **2014**, *14*, 4661−4678.
(12) Platt, S. M.; El Haddad, I.; Pieber, S. M.; Zardini, A. A.; Suarez-Bertoa, R.; Clairotte, M.; Daellenbach, K. R.; Huang, R. J.; Slowik, J. G.; Hellebust, S.; Temime-Roussel, B.; Marchand, N.; de Gouw, J.; Jimenez, J. L.; Hayes, P. L.; Robinson, A. L.; Baltensperger, U.; Astorga, C.; Prevot, A. S. H. Gasoline cars produce more carbonaceous particulate matter than modern filter-equipped diesel cars. *Sci. Rep.* **2017**, *7*, No. 4926.
(13) Zhao, Y. L.; Lambe, A. T.; Saleh, R.; Saliba, G.; Robinson, A. L. Secondary organic aerosol production from gasoline vehicle exhaust: Effects of engine technology, cold start, and emission certification standard. *Environ. Sci. Technol.* **2018**, *52*, 1253−1261.
(14) Pieber, S. M.; Kumar, N. K.; Klein, F.; Comte, P.; Bhattu, D.; Dommen, J.; Bruns, E. A.; Kilic, D.; El Haddad, I.; Keller, A.; Czerwinski, J.; Heeb, N.; Baltensperger, U.; Slowik, J. G.; Prevot, A. S. H. Gas-phase composition and secondary organic aerosol formation from standard and particle filter-retrofitted gasoline direct injection vehicles investigated in a batch and flow reactor. *Atmos. Chem. Phys.* **2018**, *18*, 9929−9954.
(15) Deng, W.; Fang, Z.; Wang, Z. Y.; Zhu, M.; Zhang, Y. L.; Tang, M. J.; Song, W.; Lowther, S.; Huang, Z. H.; Jones, K.; Peng, P. A.; Wang, X. M. Primary emissions and secondary organic aerosol formation from in-use diesel vehicle exhaust: Comparison between idling and cruise mode. *Sci. Total Environ.* **2020**, *699*, No. 134357.
(16) Tkacik, D. S.; Lambe, A. T.; Jathar, S.; Li, X.; Presto, A. A.; Zhao, Y. L.; Blake, D.; Meinardi, S.; Jayne, J. T.; Croteau, P. L.; Robinson, A. L. Secondary organic aerosol formation from in-use motor vehicle emissions using a potential aerosol mass reactor. *Environ. Sci. Technol.* **2014**, *48*, 11235−11242.
(17) Saha, P. K.; Reece, S. M.; Grieshop, A. P. Seasonally varying secondary organic aerosol formation from in-situ oxidation of near-highway air. *Environ. Sci. Technol.* **2018**, *52*, 7192−7202.
(18) Liu, T. Y.; Zhou, L. Y.; Liu, Q. Y.; Lee, B. P.; Yao, D. W.; Lu, H. X.; Lyu, X. P.; Guo, H.; Chan, C. K. Secondary organic aerosol formation from urban roadside air in Hong Kong. *Environ. Sci. Technol.* **2019**, *53*, 3001−3009.
(19) Wang, M.; Zhu, T.; Zheng, J.; Zhang, R. Y.; Zhang, S. Q.; Xie, X. X.; Han, Y. Q.; Li, Y. Use of a mobile laboratory to evaluate changes in on-road air pollutants during the Beijing 2008 Summer Olympics. *Atmos. Chem. Phys.* **2009**, *9*, 8247−8263.
(20) Lambe, A.; Massoli, P.; Zhang, X.; Canagaratna, M.; Nowak, J.; Daube, C.; Yan, C.; Nie, W.; Onasch, T.; Jayne, J.; Kolb, C.; Davidovits, P.; Worsnop, D.; Brune, W. Controlled nitric oxide production via O(D-1) + N2O reactions for use in oxidation flow reactor studies. *Atmos. Meas. Tech.* **2017**, *10*, 2283−2298.
(21) Peng, Z.; Palm, B. B.; Day, D. A.; Talukdar, R. K.; Hu, W. W.; Lambe, A. T.; Brune, W. H.; Jimenez, J. L. Model evaluation of new techniques for maintaining high-NO conditions in oxidation flow reactors for the study of OH-initiated atmospheric chemistry. *ACS Earth Space Chem.* **2018**, *2*, 72−86.
(22) Zheng, Y.; Cheng, X.; Liao, K. R.; Li, Y. W.; Li, Y. J.; Hu, W. W.; Liu, Y.; Zhu, T.; Chen, S. Y.; Zeng, L. M.; Worsnop, D.; Chen, Q.; Huang, R. J. Characterization of anthropogenic organic aerosols by TOF-ACSM with the new capture vaporizer. *Atmos. Meas. Tech.* **2020**, *13*, 2457−2472.
(23) Huang, G. C.; Liu, Y.; Shao, M.; Li, Y.; Chen, Q.; Zheng, Y.; Wu, Z. J.; Liu, Y. C.; Wu, Y. S.; Hu, M.; Li, X.; Lu, S. H.; Wang, C. J.; Liu, J. Y.; Zheng, M.; Zhu, T. Potentially important contribution of gas-phase oxidation of naphthalene and methylnaphthalene to secondary organic aerosol during haze events in Beijing. *Environ. Sci. Technol.* **2019**, *53*, 1235−1244.
(24) Yuan, B.; Koss, A. R.; Warneke, C.; Coggon, M.; Sekimoto, K.; de Gouw, J. A. Proton-transfer-reaction mass spectrometry: Applications in atmospheric sciences. *Chem. Rev.* **2017**, *117*, 13187−13229.
(25) Li, R.; Palm, B. B.; Ortega, A. M.; Hlywiak, J.; Hu, W. W.; Peng, Z.; Day, D. A.; Knote, C.; Brune, W. H.; de Gouw, J. A.; Jimenez, J. L. Modeling the radical chemistry in an oxidation flow reactor: radical formation and recycling, sensitivities, and the OH exposure estimation equation. *J. Phys. Chem. A* **2015**, *119*, 4418−4432.
(26) Mao, J.; Ren, X.; Brune, W. H.; Olson, J. R.; Crawford, J. H.; Fried, A.; Huey, L. G.; Cohen, R. C.; Heikes, B.; Singh, H. B.; Blake, D. R.; Sachse, G. W.; Diskin, G. S.; Hall, S. R.; Shetter, R. E. Airborne measurement of OH reactivity during INTEX-B. *Atmos. Chem. Phys.* **2009**, *9*, 163−173.
(27) Peng, Z.; Day, D. A.; Ortega, A. M.; Palm, B. B.; Hu, W. W.; Stark, H.; Li, R.; Tsigaridis, K.; Brune, W. H.; Jimenez, J. L. Non-OH chemistry in oxidation flow reactors for the study of atmospheric chemistry systematically examined by modeling. *Atmos. Chem. Phys.* **2016**, *16*, 4283−4305.
(28) De Gouw, J.; Jimenez, J. L. Organic aerosols in the earth's atmosphere. *Environ. Sci. Technol.* **2009**, *43*, 7614−7618.
(29) DeCarlo, P. F.; Ulbrich, I. M.; Crounse, J.; de Foy, B.; Dunlea, E. J.; Aiken, A. C.; Knapp, D.; Weinheimer, A. J.; Campos, T.; Wennberg, P. O.; Jimenez, J. L. Investigation of the sources and processing of organic aerosol over the Central Mexican Plateau from aircraft measurements during MILAGRO. *Atmos. Chem. Phys.* **2010**, *10*, 5257−5280.
(30) de Gouw, J. A.; Brock, C. A.; Atlas, E. L.; Bates, T. S.; Fehsenfeld, F. C.; Goldan, P. D.; Holloway, J. S.; Kuster, W. C.; Lerner, B. M.; Matthew, B. M.; Middlebrook, A. M.; Onasch, T. B.; Peltier, R. E.; Quinn, P. K.; Senff, C. J.; Stohl, A.; Sullivan, A. P.; Trainer, M.; Warneke, C.; Weber, R. J.; Williams, E. J. Sources of particulate matter in the northeastern United States in summer: 1. Direct emissions and secondary formation of organic matter in urban plumes. *J. Geophys. Res.* **2008**, *113*, No. 19.
(31) Odum, J. R.; Hoffmann, T.; Bowman, F.; Collins, D.; Flagan, R. C.; Seinfeld, J. H. Gas/particle partitioning and secondary organic aerosol yields. *Environ. Sci. Technol.* **1996**, *30*, 2580−2585.
(32) Derwent, R. G.; Jenkin, M. E.; Utembe, S. R.; Shallcross, D. E.; Murrells, T. P.; Passant, N. R. Secondary organic aerosol formation from a large number of reactive man-made organic compounds. *Sci. Total Environ.* **2010**, *408*, 3374−3381.
(33) Grosjean, D.; Seinfeld, J. H. Parameterization of the formation potential of secondary organic aerosols. *Atmos. Environ.* **1989**, *23*, 1733−1747.
(34) Sun, Y. L.; Du, W.; Fu, P. Q.; Wang, Q. Q.; Li, J.; Ge, X. L.; Zhang, Q.; Zhu, C. M.; Ren, L. J.; Xu, W. Q.; Zhao, J.; Han, T. T.; Worsnop, D. R.; Wang, Z. F. Primary and secondary aerosols in Beijing in winter: sources, variations and processes. *Atmos. Chem. Phys.* **2016**, *16*, 8309−8329.
(35) Li, K.; Li, J. L.; Tong, S. R.; Wang, W. G.; Huang, R. J.; Ge, M. F. Characteristics of wintertime VOCs in suburban and urban Beijing: concentrations, emission ratios, and festival effects. *Atmos. Chem. Phys.* **2019**, *19*, 8021−8036.
(36) Meng, Z.; Wu, L.; Xu, X.; Xu, W.; Zhang, R.; Jia, X.; Liang, L.; Miao, Y.; Cheng, H.; Xie, Y.; He, J.; Zhong, J. Changes in ammonia

https://doi.org/10.1021/acs.est.0c08591
Environ. Sci. Technol. XXXX, XXX, XXX−XXX

and its effects on PM2.5 chemical property in three winter seasons in Beijing, China. *Sci. Total Environ.* **2020**, *749*, No. 142208.
(37) Zheng, B.; Tong, D.; Li, M.; Liu, F.; Hong, C. P.; Geng, G. N.; Li, H. Y.; Li, X.; Peng, L. Q.; Qi, J.; Yan, L.; Zhang, Y. X.; Zhao, H. Y.; Zheng, Y. X.; He, K. B.; Zhang, Q. Trends in China's anthropogenic emissions since 2010 as the consequence of clean air actions. *Atmos. Chem. Phys.* **2018**, *18*, 14095−14111.
(38) Li, H. Y.; Cheng, J.; Zhang, Q.; Zheng, B.; Zhang, Y. X.; Zheng, G. J.; He, K. B. Rapid transition in winter aerosol composition in Beijing from 2014 to 2017: response to clean air actions. *Atmos. Chem. Phys.* **2019**, *19*, 11485−11499.
(39) Li, Y. J.; Sun, Y.; Zhang, Q.; Li, X.; Li, M.; Zhou, Z.; Chan, C. K. Real-time chemical characterization of atmospheric particulate matter in China: A review. *Atmos. Environ.* **2017**, *158*, 270−304.
(40) Cheng, X.; Li, H.; Zhang, Y. J.; Li, Y. P.; Zhang, W. Q.; Wang, X. Z.; Bi, F.; Zhang, H.; Gao, J.; Chai, F. H.; Lun, X. X.; Chen, Y. Z.; Gao, J.; Lv, J. Y. Atmospheric isoprene and monoterpenes in a typical urban area of Beijing: Pollution characterization, chemical reactivity and source identification. *J. Environ. Sci.* **2018**, *71*, 150−167.
(41) Dai, T. Y.; Wang, W.; Ren, L. H.; Chen, J. H.; Liu, H. J. Emissions of non-methane hydrocarbons from cars in China. *Sci. China: Chem.* **2010**, *53*, 263−272.
(42) Liu, Y.; Shao, M.; Zhang, J.; Fu, L. L.; Lu, S. H. Distributions and source apportionment of ambient volatile organic compounds in Beijing city, China. *J. Environ. Sci. Health, Part A: Toxic/Hazard. Subst. Environ. Eng.* **2005**, *40*, 1843−1860.
(43) Barletta, B.; Meinardi, S.; Rowland, F. S.; Chan, C. Y.; Wang, X. M.; Zou, S. C.; Chan, L. Y.; Blake, D. R. Volatile organic compounds in 43 Chinese cities. *Atmos. Environ.* **2005**, *39*, 5979−5990.
(44) Liu, J. F.; Mu, Y. J.; Zhang, Y. J.; Zhang, Z. M.; Wang, X. K.; Liu, Y. J.; Sun, Z. Q. Atmospheric levels of BTEX compounds during the 2008 Olympic Games in the urban area of Beijing. *Sci. Total Environ.* **2009**, *408*, 109−116.
(45) Sun, J.; Wu, F. K.; Hu, B.; Tang, G. Q.; Zhang, J. K.; Wang, Y. S. VOC characteristics, emissions and contributions to SOA formation during hazy episodes. *Atmos. Environ.* **2016**, *141*, 560−570.
(46) McDonald, B. C.; de Gouw, J. A.; Gilman, J. B.; Jathar, S. H.; Akherati, A.; Cappa, C. D.; Jimenez, J. L.; Lee-Taylor, J.; Hayes, P. L.; McKeen, S. A.; Cui, Y. Y.; Kim, S. W.; Gentner, D. R.; Isaacman-VanWertz, G.; Goldstein, A. H.; Harley, R. A.; Frost, G. J.; Roberts, J. M.; Ryerson, T. B.; Trainer, M. Volatile chemical products emerging as largest petrochemical source of urban organic emissions. *Science* **2018**, *359*, 760−764.
(47) Sun, K.; Tao, L.; Miller, D. J.; Pan, D.; Golston, L. M.; Zondlo, M. A.; Griffin, R. J.; Wallace, H. W.; Leong, Y. J.; Yang, M. M.; Zhang, Y.; Mauzerall, D. L.; Zhu, T. Vehicle emissions as an important urban ammonia source in the United States and China. *Environ. Sci. Technol.* **2017**, *51*, 2472−2481.
(48) Nenes, A.; Pandis, S. N.; Weber, R. J.; Russell, A. Aerosol pH and liquid water content determine when particulate matter is sensitive to ammonia and nitrate availability. *Atmos. Chem. Phys.* **2020**, *20*, 3249−3258.
(49) Ortega, A. M.; Hayes, P. L.; Peng, Z.; Palm, B. B.; Hu, W. W.; Day, D. A.; Li, R.; Cubison, M. J.; Brune, W. H.; Graus, M.; Warneke, C.; Gilman, J. B.; Kuster, W. C.; de Gouw, J.; Gutierrez-Montes, C.; Jimenez, J. L. Real-time measurements of secondary organic aerosol formation and aging from ambient air in an oxidation flow reactor in the Los Angeles area. *Atmos. Chem. Phys.* **2016**, *16*, 7411−7433.
(50) Liu, J.; Chu, B. W.; Chen, T. Z.; Liu, C. G.; Wang, L.; Bao, X. L.; He, H. Secondary organic aerosol formation from ambient air at an urban site in Beijing: effects of OH exposure and precursor concentrations. *Environ. Sci. Technol.* **2018**, *52*, 6834−6841.
(51) Shah, R. U.; Coggon, M. M.; Gkatzelis, G. I.; McDonald, B. C.; Tasoglou, A.; Huber, H.; Gilman, J.; Warneke, C.; Robinson, A. L.; Presto, A. A. Urban oxidation flow reactor measurements reveal significant secondary organic aerosol contributions from volatile emissions of emerging importance. *Environ. Sci. Technol.* **2020**, *54*, 714−725.
(52) Palm, B. B.; Campuzano-Jost, P.; Ortega, A. M.; Day, D. A.; Kaser, L.; Jud, W.; Karl, T.; Hansel, A.; Hunter, J. F.; Cross, E. S.; Kroll, J. H.; Peng, Z.; Brune, W. H.; Jimenez, J. L. In situ secondary organic aerosol formation from ambient pine forest air using an oxidation flow reactor. *Atmos. Chem. Phys.* **2016**, *16*, 2943−2970.
(53) Palm, B. B.; de Sa, S. S.; Day, D. A.; Campuzano-Jost, P.; Hu, W. W.; Seco, R.; Sjostedt, S. J.; Park, J. H.; Guenther, A. B.; Kim, S.; Brito, J.; Wurm, F.; Artaxo, P.; Thalman, R.; Wang, J.; Yee, L. D.; Wernis, R.; Isaacman-VanWertz, G.; Goldstein, A. H.; Liu, Y. J.; Springston, S. R.; Souza, R.; Newburn, M. K.; Alexander, M. L.; Martin, S. T.; Jimenez, J. L. Secondary organic aerosol formation from ambient air in an oxidation flow reactor in central Amazonia. *Atmos. Chem. Phys.* **2018**, *18*, 467−493.
(54) Kroll, J. H.; Smith, J. D.; Che, D. L.; Kessler, S. H.; Worsnop, D. R.; Wilson, K. R. Measurement of fragmentation and functionalization pathways in the heterogeneous oxidation of oxidized organic aerosol. *Phys. Chem. Chem. Phys.* **2009**, *11*, 8005−8014.
(55) Lambe, A. T.; Onasch, T. B.; Croasdale, D. R.; Wright, J. P.; Martin, A. T.; Franklin, J. P.; Massoli, P.; Kroll, J. H.; Canagaratna, M. R.; Brune, W. H.; Worsnop, D. R.; Davidovits, P. Transitions from functionalization to fragmentation reactions of laboratory secondary organic aerosol (SOA) generated from the OH oxidation of alkane precursors. *Environ. Sci. Technol.* **2012**, *46*, 5430−5437.
(56) Chen, Q.; Heald, C. L.; Jimenez, J. L.; Canagaratna, M. R.; Zhang, Q.; He, L. Y.; Huang, X. F.; Campuzano-Jost, P.; Palm, B. B.; Poulain, L.; Kuwata, M.; Martin, S. T.; Abbatt, J. P. D.; Lee, A. K. Y.; Liggio, J. Elemental composition of organic aerosol: The gap between ambient and laboratory measurements. *Geophys. Res. Lett.* **2015**, *42*, 4182−4189.
(57) Robinson, A. L.; Grieshop, A. P.; Donahue, N. M.; Hunt, S. W. Updating the conceptual model for fine particle mass emissions from combustion systems. *J. Air Waste Manage. Assoc.* **2010**, *60*, 1204−1222.
(58) George, I. J.; Hays, M. D.; Herrinton, J. S.; Preston, W.; Snow, R.; Faircloth, J.; George, B. J.; Long, T.; Baldauf, R. W. Effects of cold temperature and ethanol content on VOC emissions from light-duty gasoline vehicles. *Environ. Sci. Technol.* **2015**, *49*, 13067−13074.
(59) Zhu, R. C.; Hu, J. N.; Bao, X. F.; He, L. Q.; Lai, Y. T.; Zu, L.; Li, Y. F.; Su, S. Tailpipe emissions from gasoline direct injection (GDI) and port fuel injection (PFI) vehicles at both low and high ambient temperatures. *Environ. Pollut.* **2016**, *216*, 223−234.
(60) Drozd, G. T.; Zhao, Y. L.; Saliba, G.; Frodin, B.; Maddox, C.; Weber, R. J.; Chang, M. C. O.; Maldonado, H.; Sardar, S.; Robinson, A. L.; Goldstein, A. H. Time resolved measurements of speciated tailpipe emissions from motor vehicles: Trends with emission control technology, cold start effects, and speciation. *Environ. Sci. Technol.* **2016**, *50*, 13592−13599.
(61) Ahlberg, E.; Eriksson, A.; Brune, W. H.; Roldin, P.; Svenningsson, B. Effect of salt seed particle surface area, composition and phase on secondary organic aerosol mass yields in oxidation flow reactors. *Atmos. Chem. Phys.* **2019**, *19*, 2701−2712.
(62) Drozd, G. T.; Zhao, Y. L.; Saliba, G.; Frodin, B.; Maddox, C.; Chang, M. C. O.; Maldonado, H.; Sardar, S.; Weber, R. J.; Robinson, A. L.; Goldstein, A. H. Detailed speciation of intermediate volatility and semivolatile organic compound emissions from gasoline vehicles: Effects of cold-starts and implications for secondary organic aerosol formation. *Environ. Sci. Technol.* **2019**, *53*, 1706−1714.
(63) Saliba, G.; Saleh, R.; Zhao, Y. L.; Presto, A. A.; Larnbe, A. T.; Frodin, B.; Sardar, S.; Maldonado, H.; Maddox, C.; May, A. A.; Drozd, G. T.; Goldstein, A. H.; Russell, L. M.; Hagen, F.; Robinson, A. L. Comparison of Gasoline Direct-Injection (GDI) and Port Fuel Injection (PFI) Vehicle Emissions: Emission Certification Standards, Cold-Start, Secondary Organic Aerosol Formation Potential, and Potential Climate Impacts. *Environ. Sci. Technol.* **2017**, *51*, 6542−6552.
(64) Peng, Z.; Jimenez, J. L. Radical chemistry in oxidation flow reactors for atmospheric chemistry research. *Chem. Soc. Rev.* **2020**, *49*, 2570−2616.

https://doi.org/10.1021/acs.est.0c08591
Environ. Sci. Technol. XXXX, XXX, XXX−XXX

(65) Hu, W. W.; Campuzano-Jost, P.; Day, D. A.; Croteau, P.; Canagaratna, M. R.; Jayne, J. T.; Worsnop, D. R.; Jimenez, J. L. Evaluation of the new capture vapourizer for aerosol mass spectrometers (AMS) through laboratory studies of inorganic species. *Atmos. Meas. Tech.* **2017**, *10*, 2897−2921.
(66) Zhao, Y. L.; Saleh, R.; Saliba, G.; Presto, A. A.; Gordon, T. D.; Drozd, G. T.; Goldstein, A. H.; Donahue, N. M.; Robinson, A. L. Reducing secondary organic aerosol formation from gasoline vehicle exhaust. *Proc. Natl. Acad. Sci. U.S.A.* **2017**, *114*, 6984−6989.
(67) Ng, N. L.; Kroll, J. H.; Keywood, M. D.; Bahreini, R.; Varutbangkul, V.; Flagan, R. C.; Seinfeld, J. H.; Lee, A.; Goldstein, A. H. Contribution of first- versus second-generation products to secondary organic aerosols formed in the oxidation of biogenic hydrocarbons. *Environ. Sci. Technol.* **2006**, *40*, 2283−2297.
(68) Pye, H. O. T.; Pouliot, G. A. Modeling the role of alkanes, polycyclic aromatic hydrocarbons, and their oligomers in secondary organic aerosol formation. *Environ. Sci. Technol.* **2012**, *46*, 6041−6047.
(69) Tang, R.; Lu, Q.; Guo, S.; Wang, H.; Song, K.; Yu, Y.; Tan, R.; Liu, K.; Shen, R.; Chen, S.; Zeng, L.; Jorga, S. D.; Zhang, Z.; Zhang, W.; Shuai, S.; Robinson, A. L. Measurement report: Distinct emissions and volatility distribution of intermediate-volatility organic compounds from on-road Chinese gasoline vehicles: implication of high secondary organic aerosol formation potential. *Atmos. Chem. Phys.* **2021**, *21*, 2569−2583.
(70) Hodzic, A.; Jimenez, J. L. Modeling anthropogenically controlled secondary organic aerosols in a megacity: a simplified framework for global and climate models. *Geosci. Model Dev.* **2011**, *4*, 901−917.
(71) Miao, R.; Chen, Q.; Zheng, Y.; Cheng, X.; Sun, Y.; Palmer, P. I.; Shrivastava, M.; Guo, J.; Zhang, Q.; Liu, Y.; Tan, Z.; Ma, X.; Chen, S.; Zeng, L.; Lu, K.; Zhang, Y. Model bias in simulating major chemical components of PM2.5 in China. *Atmos. Chem. Phys.* **2020**, *20*, 12265−12284.
(72) Zheng, B.; Huo, H.; Zhang, Q.; Yao, Z. L.; Wang, X. T.; Yang, X. F.; Liu, H.; He, K. B. High-resolution mapping of vehicle emissions in China in 2008. *Atmos. Chem. Phys.* **2014**, *14*, 9787−9805.
(73) Duan, J.; Huang, R. J.; Lin, C. S.; Dai, W. T.; Wang, M.; Gu, Y. F.; Wang, Y.; Zhong, H. B.; Zheng, Y.; Ni, H. Y.; Dusek, U.; Chen, Y.; Li, Y. J.; Chen, Q.; Worsnop, D. R.; O'Dowd, C. D.; Cao, J. J. Distinctions in source regions and formation mechanisms of secondary aerosol in Beijing from summer to winter. *Atmos. Chem. Phys.* **2019**, *19*, 10319−10334.
(74) Ma, X. F.; Tan, Z. F.; Lu, K. D.; Yang, X. P.; Liu, Y. H.; Li, S. L.; Li, X.; Chen, S. Y.; Novelli, A.; Cho, C. M.; Zeng, L. M.; Wahner, A.; Zhang, Y. H. Winter photochemistry in Beijing: Observation and model simulation of OH and HO2 radicals at an urban site. *Sci. Total Environ.* **2019**, *685*, 85−95.
(75) Woodward-Massey, R.; Slater, E. J.; Alen, J.; Ingham, T.; Cryer, D. R.; Stimpson, L. M.; Ye, C. X.; Seakins, P. W.; Whalley, L. K.; Heard, D. E. Implementation of a chemical background method for atmospheric OH measurements by laser-induced fluorescence: Characterisation and observations from the UK and China. *Atmos. Meas. Tech.* **2020**, *13*, 3119−3146.
(76) Li, X.; Dallmann, T. R.; May, A. A.; Stanier, C. O.; Grieshop, A. P.; Lipsky, E. M.; Robinson, A. L.; Presto, A. A. Size distribution of vehicle emitted primary particles measured in a traffic tunnel. *Atmos. Environ.* **2018**, *191*, 9−18.

https://doi.org/10.1021/acs.est.0c08591
Environ. Sci. Technol. XXXX, XXX, XXX−XXX